Imaging a Solvent-Swollen Polymer Gel Network by Open Liquid Transmission Electron Microscopy

Satyam Srivastava[1], Alexander E. Ribbe [1], Thomas P Russell [*1,2,3], David A Hoagland[*1]

[1]Department of Polymer Science and Engineering, University of Massachusetts Amherst, Amherst, Massachusetts 01003, United States

[2]Materials Sciences Division, Lawrence Berkeley National Laboratory, Berkeley, California 94720, United States

[3]Advanced Institute for Materials Research (WPI-AIMR), Tohoku University, 2-1-1 Katahira, Aoba, Sendai 980-8577, Japan

Correspondence to: David A Hoagland (E-mail: *hoagland@mail.pse.umass.edu*) and Thomas P Russell (E-mail: *russell@mail.pse.umass.edu*)

Keywords: ((polymer gels, poly(ethylene glycol), transmission electron microscopy, ionic liquids; physical gels))

((Abstract: Visualizing the network of a solvent-swollen polymer gel remains problematic. To address this challenge, open transmission electron microscopy (TEM) was applied to thin gel films permeated by a nonvolatile ionic liquid. The targeted physical gels were prepared by cooling concentrated solutions of poly(ethylene glycol) in 1-ethyl-3-methyl imidazolium ethyl sulfate [EMIM][EtSO4]. During the cooling, gelation occurred by a frustrated crystallization of the dissolved polymer, leading to a percolated, solvent-permeated semicrystalline network in which nanoscale polymer crystals acted as crosslinks. Crystalline features ranging from ~5 to ~200 nm were observed, with the visible network strands dominantly consisting of long curvilinear crystallites of ~15-20 nm diameter. Nascent spherulites irregularly decorated the network, creating a complex structural hierarchy that complicated analyses. Lacking diffraction contrast, TEM did not visualize the many disordered, fully solvated PEG chains present in the voids between crystals. Recognizing that a network's three dimensionality is ambiguous when assessed through two-dimensional microscopy projections, a small gel region was studied by TEM tomography, revealing a nearly isotropic three-dimensional

arrangement of the curvilinear crystallites, which displayed remarkably uniform cylindrical cross sections.))

1. Introduction

The network of a gel dictates its mechanical and transport properties. However, mapping a gel across the size range of network features, spanning from the nanoscale to the microscale, poses immense challenges, due to the softness of the network, as well as its complex, statistical, and three-dimensional nature. In this investigation, open liquid transmission electron microscopy (TEM)[1] was used to visualize gel networks swollen by an ionic liquid (IL). Because of IL nonvolatility, unlike gels prepared with more ordinary (i.e., volatile) solvents, specimens were stable against TEM vacuum. An earlier publication[2] outlined how ILs can be gelled by thermally quenching relatively concentrated solutions of a crystallizable polymer, a scheme underscoring many technologically important polymer physical gels. During cooling, chains are trapped between nanoscale crystalline and solvent-swollen amorphous regions, framing a complex nanoscale percolating network. Beyond insensitivity to vacuum, the IL gels had other attributes beneficial to TEM imaging: relatively rigidity, which suppressed thermal fluctuations of the structure, and electron diffraction, which provided good imaging contrast for the crystalline features of the network. The gels were also probed by X-ray scattering to confirm the sizes/shapes of the local structural elements of the network.

Solvent-swollen gel networks have commonly been characterized by X-ray[3-6], neutron[7-9] and light scattering[10-13]. Such methods provide space– and usually time–averaged information about the network. However, because the materials are inevitably disordered, the garnered information is incomplete[3]. For example, unlike direct visualization, scattering data cannot

discern how local structures depart from the ensemble-averaged structure. In addition, scattering measurements fail to reveal network connectivity. Microscopy methods address these issues, but traditional optical microscopy lacks the needed spatial resolution, and super-resolution optical microscopy requires chemical modifications[14]. Both methods are highly limited in their ability to probe three dimensionality or dynamics. As a result, network connectivity is typically only coarsely characterized by macroscopic rheology measurements[15-17].

Electron microscopy offers the spatial and temporal resolutions needed to probe nanoscale gel structural variations, dynamics, and connectivity. Unfortunately, the accompanying exposure to high vacuum seriously complicates *in situ* visualization of gels swollen/wetted by traditional, finite vapor pressure solvents[18-22]. Consequently, solvent-swollen gels have never been imaged by TEM or scanning electron microscopy (SEM). Instead, these methods have usually been performed after exchanging the solvent, drying or fixing the new solvent, sectioning the solidified gel by microtomy, and staining the solid sections for contrast. Alternatively, the first steps can be replaced by plunge freezing followed by cryo-TEM or cryo-SEM. Both preparations potentially alter network structure[19-24], and insights into gel dynamics, as well as into the motions of any trapped diffusing species, are lost. Nevertheless, structural insights from electron microscopy have mostly tracked with those from scattering[3].

ILs, salts that melt close to or below room temperature, are typically nonvolatile. Availability of these solvents opens prospects for TEM or SEM imaging of different sorts of solvent-wetted soft materials. Even more, ILs are not just stable against evaporation at high vacuum, they possess properties conducive to the imaging, such as modest conductivity and high viscosity[1,25-27]. A diverse IL library is available, offering a wide range of solvency properties. In particular, the crystallization of concentrated poly(ethylene glycol) in the IL 1-

ethyl-3-methylimidazolium ethyl sulfate ([EMIM][$EtSO_4$]) is known to produce thermo-reversible soft gels, which have been characterized by rheological, scattering, and thermal methods[2]. Open EM imaging enabled by ILs previously facilitated investigations of diffusion dynamics of block copolymer micelles and polymer-coated nanoparticles dispersed in a liquid film or at a liquid surface[25-29]. Further, both small molecule and polymer crystals in IL have been imaged by open TEM[1,30-31].

Gelation of a solution by the crystallization of a dissolved polymer occurs for numerous polymer-solvent pairs[32-36], and the resulting networks have been visualized by cryo-SEM[37] and cryo-TEM[23] after the specimen preparations outlined above. Images revealed possibly interconnected fiber-like crystallites[23,37]. These physical gels are generally stiffer and much more heterogeneous in network structure than chemical crosslinked gels made from flexible polymers. Nevertheless, these materials display characteristic gel-like features such as (i) high solvent content (>50% by volume), (ii) frequency-invariant modulus at low frequency (reflecting the presence of a percolating stress-conveying network), (iii) significant changes to swelling when solvency conditions are altered, (iv) network features at the nanoscale, and (v) facile storage/release/transport of confined solutes. The degree of crystallinity of the polymeric component varies widely, but uncrystallized polymer is present to bridge the crystallites while keeping the network soft and swellable. In most instances the gels are reasonably transparent, reflecting dominantly nanoscale structuring, but heterogeneities such as large voids/crystals sometimes cause turbidity.

As a first step in developing nanoscale microscopy tools suited to soft, wet materials, this investigation targeted easily prepared IL gels possessing properties anticipated to be beneficial to direct *in situ* TEM imaging. While not of technological significance, these IL gels resemble in preparation and properties many hydrogels that do. Unlike past electron microscopy gel

studies, the goal was to visualize the network structure *without first solidifying the solvent*, a process likely to perturb this structure. By sorting out issues such as contrast, beam damage, and ability to reveal three-dimensional connectivity, prospects for similar TEM imaging of other gel systems can *a priori* be foreseen and assessed.

2. Results and Discussion

2.1. TEM imaging of a gel network

Due to IL hydrophilicity, the PEG solutions tended to de-wet their hydrophobic carbon supports, and consequently, most regions of a gel film were too thick for electron transmission. Nevertheless, suitable areas could be identified through the visibility of network features. As reported previously,[1,38-39] at the chosen TEM imaging conditions many neat ILs solidify after lengthy (~5-10 s) electron beam exposures. Solidification can be deduced from a slowing down and eventual arrest of motion for well-dispersed solutes, such as nanoparticles and polymer micelles, presumably because of radiolysis-induced IL crosslinking. The TEM beam exposures here, typically $\lesssim$1 s, would not be expected to cause solidification, but even longer exposures did not discernably affect the gel features visualized. TEM tomography entails larger electron doses, and, in these experiments, localized beam damage was noted; nevertheless, most regions of the imaged network showed no evidence of beam-induced damage or alteration of structure.

To prevent unconnected PEG single crystals from forming during cooling and to improve the reproducibility of imaged features, two heating/cooling steps were included in specimen preparation, steps that eliminated residual water. ([EMIM][$EtSO_4$] is highly hygroscopic.) **Figure 1(a)** shows a representative TEM image of a 3 μm x 3 μm gel region; the

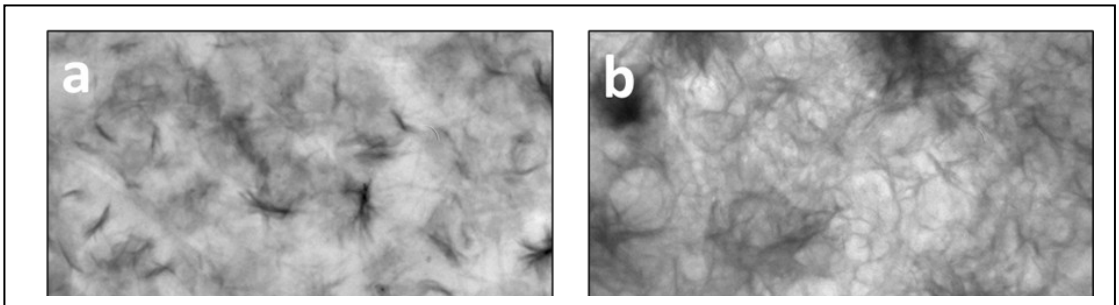

char , or

simi is

resp nm.

Crystallinity is prominently manifested as scattered 200-500 nm "wispy" dark regions surrounded by a lighter background that extends across the rest of the image. Both dark and background regions exhibited a mesh of fine curvilinear features. The dark regions consisted of clusters of coarse, irregular fibrils often splayed at both ends.

Figure 1(b) shows at higher magnification a different region of the same specimen. The dark and background regions are again easily discerned, and compared to **Figure 1(a)**, the fine curvilinear features are more evident. These features are PEG crystallites $\lesssim$15 nm in width and >100-200 nm in length. Some fine curvilinear crystallites traverse between the dark and background regions.

To explore the structure of **Figure 1(b)** further, **Figures 2(a)** and **(b**) show dark and light (background) regions from areas in the middle of **Figure 1(b)** after digital magnification and contrast enhancement. The packing of crystalline features in the dark region is clearly higher than in the background region, with the former region's coarser fibrils often too overlapped to distinguish from each other; comparable fibrils rarely decorate the background region. These images demonstrate that the PEG crystallizes predominately as either a cluster of coarse fibrils or a mesh of finer curvilinear crystallites.

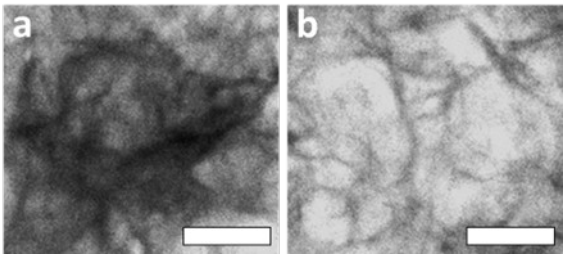

Figure 2**:** Magnified images of a) dark and b) background regions. Scale bars: 100 nm.

2.2. Image analysis

The background mesh of **Figure 1(b)** hints of a network comprised mostly of thinner curvilinear PEG crystallites. However, structures within the denser regions lacked clarity. A linear contrast adjustment was thus applied, transforming **Figure 1b** to **Figure 3a**, making both coarse fibrils and curvilinear crystallites more distinct. To isolate connected structures, binarization was needed, but maintaining a constant binarization threshold across dense and background regions worked poorly. Therefore, this threshold was calculated locally[40] as $t \times \mu_{local}$, where the t was between 0 and 1, and μ_{local} was the mean intensity of the 128 pixel x 128 pixel region surrounding a given pixel. Parameter t was changed until all crystallites in an image were satisfactorily distinguished, their dimensions unchanged from the raw image, achieved best with t=0.63. Isolated dark or bright regions of areas less than 2 pixel² (or 1 nm²) were discarded as background noise. These steps effectively isolated network features in both dense and background regions and established the structural connectivities across a full image seen in **Figures 3b** and **3c**.

Figure 3(b) colorizes **Figure 3(a)** according to crystal connectivity, creating the apparent percolating network drawn in blue; the image's non-percolating networks are drawn in green. Since nearly all the colored features are blue, a single apparent sample-spanning network incorporated most of the crystalline regions. Percolation was observed in the same manner

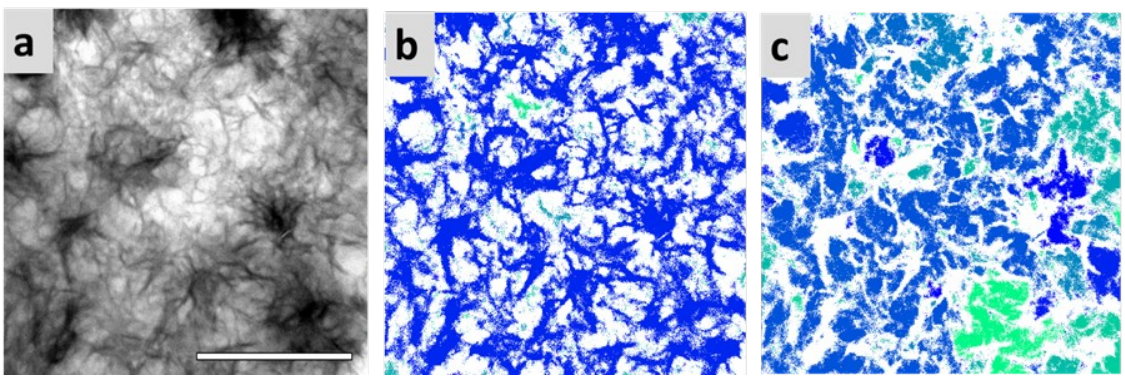

Figure 3: Figure 1(b) after: (a) contrast enhancement, (b) image segmentation highlighting polymer crystallites and their percolation, and (c) image segmentation highlighting non-crystalline regions and their percolation (regions containing disordered

consistently in images collected from across the sample. An important caveat is that TEM offers a two-dimensional projection of a three-dimensional structure, so actual connectivity cannot be established unambiguously in the manner described. In projection, elements in thicker regions will appear denser and thus more connected than those in thinner regions.

As a complement to **Figure 3(b)**, **Figure 3(c)** colorizes **Figure 3(a)** according to the connectivity of non-crystalline regions, i.e., of open spaces or voids. Alongside solvent, these regions likely hosted unseen small crystallites ($\lesssim$4 nm) and disordered polymer chains. **Figure S1** plots the distribution of largest dimension (i.e., maximum span) for void regions, which varied in size from ~12 to ~60 nm. Unsurprisingly no void percolated the entire 1200 nm x 1200 image area. The distribution of largest void size is nearly an exponential decay characterized by a mean largest dimension of ~20 nm. According to the standard scaling depiction of a random gel[41], the network correlation length ξ is given,

$$\xi \cong a\Phi^{-3/4}$$

A flexible polymer segment length, *a,* is ~2 nm, and so if the volume fraction Φ is ~0.1, ξ is ~10 nm. Here, because the network is stiffened by the physical association between chains, ξ is larger. Thus, the ~20 nm void size is within expectation for the 10% physical gel. Again, connectivity and size in three dimensions cannot unambiguously be determined from a two-

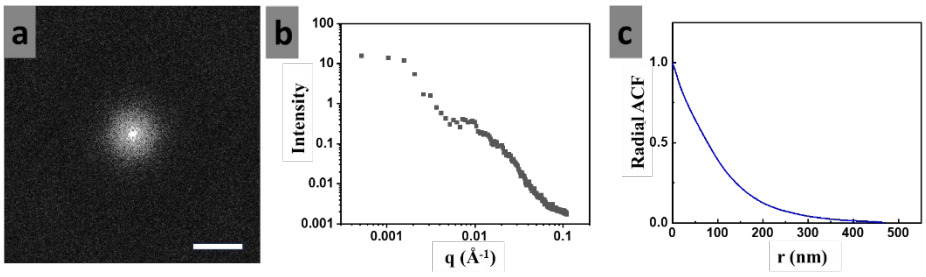

Figure 4**:** Analyses of **Figure 1(b)**: (a) Fast Fourier transform, (b) radially averaged power spectral density function, and (c) radially averaged autocorrelation function. Scale bar: 0.1 Å^{-1}.

dimensional projection; network and voids of a three-dimensional gel are inherently both percolating, trends that do not carry over into two dimensions.

In **Figure 4(a),** the two-dimensional fast Fourier transform of the raw image in **Figure 1(b)** is shown, giving little immediate indication of characteristic network feature sizes. **Figure 4(b)** shows the corresponding radially averaged power spectral density function (PSDF), and unsurprisingly, there are no prominent peak(s) indicating a characteristic size(s). A small shoulder at q~0.005 Å^{-1} indicates the slight preference for ~120 nm-diameter darker regions. These regions appear randomly placed in the lighter background. The accompanying radially averaged auto-correlation function (ACF)[42] is shown in **Figure 4(c)**. The ACF was obtained as the inverse Fourier transform of the two-dimensional PSDF of the image in **Figure 1(b)**[42]. The radially averaged ACF can be fit as an exponential decay with a correlation length of ~104 nm, close to the length extracted from the PSDF (**Figure S2**).

2.3. X-ray scattering

The PSDF calculated from a phase contrast optical microscope image is sometime comparable to the same x-ray scattering pattern of the material, as the two experiments probe microstructure similarly[42]. For a TEM image, the analogous comparison is less certain, as

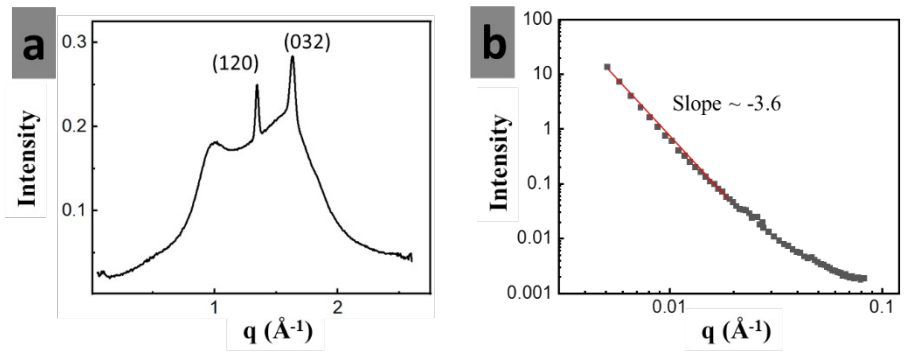

Figure 5**:** Radially averaged (a) wide and (b) small angle x-ray scattering patterns of a bulk gel.

contrast now comes from mass-thickness, electron diffraction, and additional mechanisms[43]. A close overlap between radially averaged PSDF and x-ray scattering pattern is not expected.

Figures 5(a) and **5(b)** show the wide and small angle x-ray scattering (WAXS and SAXS) patterns obtained from a thin gel film, respectively. A prior DSC study found that a similarly prepared PEG-IL gel had a lower degree of PEG crystallinity (~55%) than neat PEG (~70%) [2]. The non-crystalline PEG is undetected by TEM or x-ray methods and is, more than likely, solvated in network voids. WAXS reflctions at $q \approx 1.35$ Å^{-1} and 1.64 Å^{-1} confirm PEG crystallinity[44-45], with these peaks corresponding to the 120 and 032* reflections of PEG's monoclinic crystalline form, respectively (*indicates intensity augmented by nearby 112, 212, 124, 204, and 004 reflections). In this crystalline form PEG chains adopt a 7_2 helix. PEG can also crystallize in a triclinic form with chains adopting a planar zig-zag conformation. The WAXS patterns of the two forms are quite similar, so **Figure 5a** does not reveal which form was adopted. The SAXS profile in **Figure 5(b)**, lacking characteristic peaks, suggests little nanoscale order. Over 0.006 Å$^{-1} < q < 0.017$ Å^{-1} the SAXS intensity dropped nearly as a power law with an exponent of ~-3.6, consistent with sharp interfaces at size scales above ~30 nm. Such scattering manifests the relatively clean edges of the larger fibrils.

2.4. TEM tomography

TEM cannot differentiate between a three-dimensional network and a dense dispersed collection of incompletely percolated objects. To distinguish the two possibilities, TEM tomography was conducted on a ~50 nm thick gel film deposited on a lacey carbon support. **Movie S1** is a tilt series image stack collecting the raw TEM images obtained at different angles for tomographic reconstruction. The prolonged beam exposure needed for the series produced visually apparent but highly localized damage in the form of open cavities. Tomography was performed well away from these cavities, as well as any dark regions, for a

background area in the middle of the stacked images where features were unaffected by beam exposure. **Movie S2** displays z-slices computed by the eTomo program of the open source IMOD tomography package available from the University of Colorado Boulder. **Movie S3** highlights the shapes of the high contrast crystal domains after suppressing noise (i.e., removing individual pixels and small pixel clusters of differing intensity inside regions of otherwise uniform intensity) and modeling the domain surfaces by manual contour line extraction using the 3dmod program of IMOD.

Figure 6 offers a representative perspective of the model, showing branched curvilinear crystallites and a percolated void space emptied of all low-contrast features. The processes of noise suppression and contour line extraction simplified the features displayed, sacrificing resolution to gain clarity into the three-dimensional arrangement and shape of crystalline features. Crystallite dimensions after reconstruction (**Movie S3**) were essentially the same as those inferred from the raw image stack (**Movie S1**). Imaging at higher magnification would require higher electron doses or longer acquisition times and consequently a greater likelihood of artefacts. Movie S1 shows that limited localized beam damage occurred even at the beam dose used, so going to higher magnification proved problematic. The crystallites, now conclusively shown to be cylindrical, are remarkably uniform in diameter, ~4 nm, and their lengths sometimes extended beyond ~50 nm, spanning most of the image box. Despite small diameters, these crystallites are examples of the same curvilinear features noted in the lower magnification, lower resolution TEM image in **Figure 1(b)**. The crystallites appear slightly clustered and aligned in the model, although these suggestions are inconclusive due to the limited size of the region modeled.

The reconstructed crystallites notably do not percolate across the tomograph nor are they much interconnected. Image processing might have erased some crystallite interconnections,

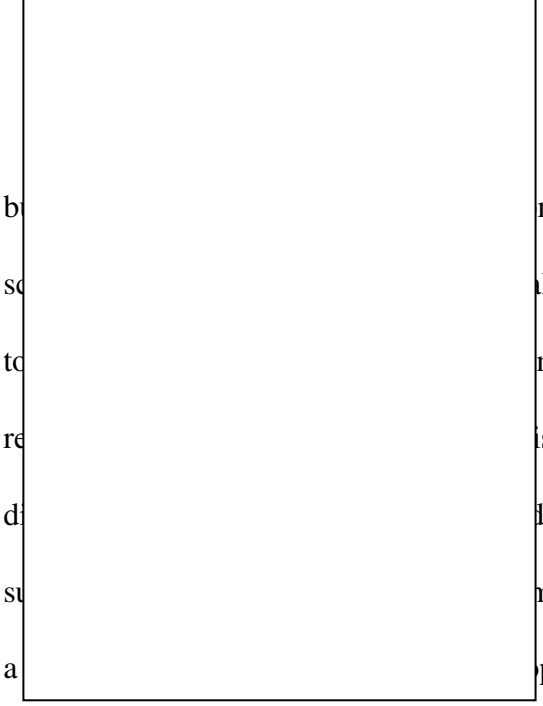

bulk mograph's neighboring crystallites much exceed the sc l change incurred during image analysis. Since the to n, the gross percolation of the crystalline network re ist, small interconnecting crystallites less than 1 nm-d luring imaging due to low contrast/finite resolution; su modynamically stable, collecting in a bundle at most a perties of the bulk material conclusively established that the films were mechanically percolated in three dimensions;[2] on a gross scale, preventing the films from flowing as liquids. The tomograph proved that the network nanostructure was three-dimensional, and while the gel was made as a thin film, this structure was nearly isotropic, i.e., the solid support did not significantly align the crystallites.

The limited spatial resolution of TEM makes a rigorous linkage of microscopy features to trends observed by WAXS and rheology extremely difficult. The latter, for example, is highly sensitive to the density of the unseen disordered chains bridging crystallites. Likewise, because of their large sizes, WAXS is highly sensitive to the relatively sparse spherulites. On a volumetric basis, the crystalline features observed by TEM roughly account for all the crystalline PEG in the gels.

2.5. Proposed Network Morphology

Neat semicrystalline polymers, especially those like PEG that are relatively flexible,[46] display a nanoscale morphology consisting of lamellar polymer crystals sporadically bridged by a low fraction of disordered chain sections called "tie" chains. The tie chains run through the amorphous polymer regions separating the lamella. A majority of the chains in a crystal fold at the lamellar surface and re-enter the same crystal from which they emerged. This morphological depiction, known as the folded chain model, is somewhat similar to the

depiction we propose here for the arrangement of chains in PEG gels, with most chains incorporated into crystals but some disordered chain section again bridging between crystals. The amorphous region of the neat materials is replaced by the apparent voids of the gels. Although not established by experiment, a few of the chains exiting a fibril likely fold and re-enter the same crystal. (The curvilinear crystallite diameter is just ~4 nm.). This model is not new: it closely resembles the historical “fringed micelle” model of neat semicrystalline polymers. In the fringed micelle model, chains are envisaged to pass axially in succession through several fibrillar crystallites. Different exiting chains at the fibril end pass to different crystals, effectively creating a stress network. Nowadays, the fringed micelle model is mostly discounted, with the folded chain, or lamellar, model confirmed for nearly all polymer systems examined.

The key differences between the two morphological models are the shape of the crystals, the presence of folds, and the direction taken by chains within the crystal. In most aspects the crystallites of these PEG gels fit the fringed micelle model. The dominant crystalline features are cylindrical, and their small diameter, ~4 nm, argues for chains aligned axially.[47] However, efforts to employ electron diffraction to determine the chain orientation in the crystallites failed due to beam damage. Also, some chains might fold tightly at fibril ends, allowing re-entry not incorporated into the model.

Past literature has hypothesized that fringe micelles are present in gels produced by polymer crystallization-induced crystallization.[47] The current PEG gels "melted" at 50-60ºC, close to the melting temperature of PEG[2]. Across the same temperature range the plateau shear modulus rose/fell by almost 5 orders of magnitude during cooling/heating cycles, demonstrating the reversible formation/disruption of a soft, percolated network of stress-conveying paths (i.e., "stress chains")[2]. These trends argue, but do not prove, the presence of

disordered interconnections, or tie chains, running between fibrils and curvilinear crystallites, features undetected by TEM due to a lack of diffraction contrast. Many such chains are necessary to explain the large modulus changes observed upon cooling/heating. Heavy element[2] labeling of single chains would be necessary to achieve the contrast need to visualize these chain sections, a skill beyond current TEM practice. It is not possible to resolve individual random polymer chains embedded in a liquid or solid matrix with any current TEM (including aberration corrected TEM) available.

The localized clusters of coarse fibrils found in the darker regions of the gel images are strongly suggested to be nascent PEG spherulites. At a slightly lower PEG concentration (0.05 mg/ml) and with slower cooling (hours rather than minutes), gelation of the films did not occur, and as seen in **Figure S3,** analogous TEM imaging instead revealed physically separated spherulitic or branched crystals of widely varied size. No thin curvilinear crystallites were observed in the regions between crystals. The spherulitic crystals strikingly resemble the structures noted in the gel's dark regions. In both cases the coarse fibrils framing the structures could be lamellar, explaining why their contrast is much greater than for the curvilinear crystallites. We previously reported that dissolved PEG cooled from a mix of ILs transformed into various fiber-like crystals,[1] although the objects grew on a solid support rather than in a bulk film.

3. Conclusions

Physical gels formed by polymer crystallization, or other nonspecific association, are common, and yet their network structures remain poorly understood; the same is true for many chemical gels made by covalently crosslinking dissolved polymers. The current work can be regarded as an initial step in the exploration of TEM techniques for imaging *in situ* the network nanostructures of these materials. Only *ex situ* or indirect TEM approaches have

been reported in the past, often with limited confidence that the obtained images accurately represented the network as swollen by solvent, i.e., in its native state. This first exploratory step was basically successful, but many obstacles were uncovered, and further developments are needed before the approach becomes either robust and/or general. Reasonable images of the network structure were obtained, but secondary assessments of this structure by other methods were hindered by the presence of extraneous gel features, i.e., the spherulites.

One significant finding, confirming previous speculations about other gels in this class, was the presence of cylindrical polymer crystallites closely conforming to the classic fringed micelle model. By readily accommodating the necessary interconnection between gel elements, this morphology may prove significant to an understanding the structures adopted by similar physical gels formed under polymer crystallization, including many of technological importance.

4. Experimental

4.1. Materials

Molecular weight 8,000 g/mol PEG was purchased from Sigma Aldrich, and [EMIM][EtSO4] were obtained from Ioli-tech GmbH. Copper TEM grids were purchased from Electron Microscopy Sciences. The grids, coated with amorphous carbon, were available in two types: continuous (no openings) and lacey (with micron-sized mesh-like openings).

4.2. TEM sample preparation and imaging

To cast gel films, 0.1 g/ml PEG was stirred in IL for 24 hours at 70°C. A drop of the hot solution was deposited onto the TEM grid, and excess solution was quickly removed by a glass rod or filter paper. The supported film was cooled to room temperature, placed under vacuum, and reheated to 70°C for 3 hr. After a second return to room temperature, the final film was placed in a vacuum oven at room temperature for 24 hr. EM was performed shortly

afterward in a JEOL JEM-2000FX TEM operated at 200 kV acceleration voltage. When ILs did not contain PEG, they did not gel, and the corresponding TEM images did not display any features. The thickness of imaged regions was ~50 nm as assessed from thickness measurements performed during tomography acquisition described in section 4.3. All TEM images were saved as 2048 pixel x 2048 pixel grayscale images on which image analysis was conducted using programs written in MATLAB.

4.3. TEM tomography

With zero-loss imaging and a 30 eV-slit width for contrast enhancement, a JEOL- JEM-2200FS microscope was used for TEM tomography. At low dose conditions, a 1-degree tilt series was acquired at 200 kV acceleration voltage, producing a stack of 110 images. The electron dose was approximately 10 e/Å^2 per frame, within the range commonly chosen for beam-sensitive materials. The total dose for the tilt series was ~1000 e/Å^2. Reconstruction was done with eTomo program of the open source IMOD tomography package available from the University of Colorado Boulder. IL film thicknesses can easily be assessed from the tomograph and additionally were measured at various free-standing sample locations using a JEOL JEM-2200FS energy-filtered TEM in electron energy loss spectroscopy (EELS) mode using a previously reported procedure[38].

4.4. X-ray scattering

A PEG solution at 70ºC was cast at the center of the opening of a 3 mm-Teflon washer placed onto a Kapton film. After cooling to induce gelation, the gel was covered with a second Kapton film. SAXS and WAXS were executed by a Ganesha SAXS-LAB instrument operated with a Cu Kα X-ray incident beam of λ=0.1542 nm wavelength. The beam was collimated with a two-aperture system, and the measurements were performed in vacuum. The sample-to-detector distance was 1050.4 mm for SAXS and 100.4 mm for WAXS, and the

calibration standard was a silver behenate standard reference material. SAXS and WAXS patterns were recorded by a two-dimensional detector (Pilatus 300K) as a function of scattering vector $q=4\pi \sin(\theta)/\lambda$, where 2θ was the scattering angle. The data acquisition time for SAXS was 30 min and for WAXS it was 10 min. The combined background scattering from solvent and Kapton films was subtracted from the collected intensity before analysis of the scattering patterns.

Acknowledgements

We acknowledge the financial support of the National Science Foundation through DMR-2104883.

Received: ((will be filled in by the editorial staff))
Revised: ((will be filled in by the editorial staff))
Published online: ((will be filled in by the editorial staff))

References

[1] Srivastava, S., Ribbe, A. E., Russell, T. P., & Hoagland, D. A. (2020). In Situ Electron Microscopy of Poly (ethylene glycol) Crystals Grown in Thin Ionic Liquids Films. *Journal of Polymer Science, 58*(3), 478-486.

[2] Harner, J. M., & Hoagland, D. A. (2010). Thermoreversible gelation of an ionic liquid by crystallization of a dissolved polymer. *The Journal of Physical Chemistry B, 114*(10), 3411-3418.

[3] Hernandez-Cerdan, P., Mansel, B. W., Leis, A., Lundin, L., & Williams, M. A. (2018). Structural analysis of polysaccharide networks by transmission electron microscopy: comparison with small-angle X-ray scattering. *Biomacromolecules, 19*(3), 989-995.

[4] Morozova, S., Coughlin, M. L., Early, J. T., Ertem, S. P., Reineke, T. M., Bates, F. S., & Lodge, T. P. (2019). Properties of chemically cross-linked methylcellulose gels. *Macromolecules, 52*(20), 7740-7748.

[5] Mischenko, N., Reynders, K., Koch, M., Mortensen, K., Pedersen, J., Fontaine, F., Graulus, R., & Reynaers, H. (1995). Small-angle x-ray and neutron scattering from bulk and oriented triblock copolymer gels. *Macromolecules, 28*(6), 2054-2062.

[6] Geissler, E., Horkay, F., & Hecht, A. M. (1991). Osmotic and scattering properties of chemically crosslinked poly (vinyl alcohol) hydrogels. *Macromolecules, 24*(22), 6006-6011.

[7] Shibayama, M., Kawakubo, K., Ikkai, F., & Imai, M. (1998). Small-angle neutron scattering study on charged gels in deformed state. *Macromolecules, 31*(8), 2586-2592.

[8] Horkay, F., Hecht, A.-M., & Geissler, E. (1994). Small angle neutron scattering in poly (vinyl alcohol) hydrogels. *Macromolecules, 27*(7), 1795-1798.
[9] Matsunaga, T., Sakai, T., Akagi, Y., Chung, U.-i., & Shibayama, M. (2009). Structure characterization of tetra-PEG gel by small-angle neutron scattering. *Macromolecules, 42*(4), 1344-1351.
[10] Morozova, S., Hamilton, P., Ravi, N., & Muthukumar, M. (2016). Development of a vitreous substitute: incorporating charges and fibrous structures in synthetic hydrogel materials. *Macromolecules, 49*(12), 4619-4626.
[11] Morozova, S., & Muthukumar, M. (2017). Elasticity at swelling equilibrium of ultrasoft polyelectrolyte gels: Comparisons of theory and experiments. *Macromolecules, 50*(6), 2456-2466.
[12] Morozova, S., Hitimana, E., Dhakal, S., Wilcox, K. G., & Estrin, D. (2021). Scattering methods for determining structure and dynamics of polymer gels. *Journal of Applied Physics, 129*(7).
[13] Rochas, C., & Geissler, E. (2014). Measurement of dynamic light scattering intensity in gels. *Macromolecules, 47*(22), 8012-8017.
[14] Nevskyi, O., & Wöll, D. (2023). 3D Super-Resolution Fluorescence Imaging of Microgels. *Annual Review of Physical Chemistry, 74*, 391-414.
[15] Winter, H. H., & Chambon, F. (1986). Analysis of linear viscoelasticity of a crosslinking polymer at the gel point. *Journal of Rheology, 30*(2), 367-382.
[16] Chambon, F., & Winter, H. H. (1987). Linear viscoelasticity at the gel point of a crosslinking PDMS with imbalanced stoichiometry. *Journal of Rheology, 31*(8), 683-697.
[17] Chambon, F., Petrovic, Z. S., MacKnight, W. J., & Winter, H. H. (1986). Rheology of model polyurethanes at the gel point. *Macromolecules, 19*(8), 2146-2149.
[18] Mears, L. L., Draper, E. R., Castilla, A. M., Su, H., Zhuola, Dietrich, B., Nolan, M. C., Smith, G. N., Doutch, J., & Rogers, S. (2017). Drying affects the fiber network in low molecular weight hydrogels. *Biomacromolecules, 18*(11), 3531-3540.
[19] Adams, D. J. (2018). Does drying affect gel networks? *Gels, 4*(2), 32.
[20] Leis, A., Øiseth, S., Crameri, S., & Lundin, L. (2013). *Visualization of carrageenan hydrogels by electron tomography*. Paper presented at the AIP Conference Proceedings.
[21] Apkarian, R. P., Wright, E. R., Seredyuk, V. A., Eustis, S., Lyon, L. A., Conticello, V. P., & Menger, F. M. (2003). In-lens cryo-high resolution scanning electron microscopy: methodologies for molecular imaging of self-assembled organic hydrogels. *Microscopy and Microanalysis, 9*(4), 286-295.
[22] Serp, D., Mueller, M., Von Stockar, U., & Marison, I. (2002). Low-temperature electron microscopy for the study of polysaccharide ultrastructures in hydrogels. I. Theoretical and technical considerations. *Biotechnology and bioengineering, 79*(3), 243-252.
[23] Yang, Y., & Geil, P. (1983). Morphology and properties of PVC/solvent gels. *Journal of Macromolecular Science, Part B: Physics, 22*(3), 463-488.
[24] Kiyama, R., Yoshida, M., Nonoyama, T., Sedlačík, T., Jinnai, H., Kurokawa, T., Nakajima, T., & Gong, J. P. (2023). Nanoscale TEM imaging of hydrogel network architecture. *Advanced Materials, 35*(1), 2208902.
[25] Kim, P. Y., Gao, Y., Chai, Y., Ashby, P. D., Ribbe, A. E., Hoagland, D. A., & Russell, T. P. (2019). Assessing pair interaction potentials of nanoparticles on liquid interfaces. *ACS nano, 13*(3), 3075-3082.
[26] Gao, Y., Kim, P. Y., Hoagland, D. A., & Russell, T. P. (2020). Bidisperse Nanospheres Jammed on a Liquid Surface. *ACS nano, 14*(8), 10589-10599.

[27] Kim, P. Y., Gao, Y., Fink, Z., Ribbe, A. E., Hoagland, D. A., & Russell, T. P. (2022). Dynamic reconfiguration of compressed 2D nanoparticle monolayers. *ACS nano, 16*(4), 5496-5506.
[28] Ueki, T., & Watanabe, M. (2007). Lower critical solution temperature behavior of linear polymers in ionic liquids and the corresponding volume phase transition of polymer gels. *Langmuir, 23*(3), 988-990.
[29] Ueki, T., & Watanabe, M. (2006). Upper critical solution temperature behavior of poly (N-isopropylacrylamide) in an ionic liquid and preparation of thermo-sensitive nonvolatile gels. *Chemistry Letters, 35*(8), 964-965.
[30] Huang, J. Y., Zhong, L., Wang, C. M., Sullivan, J. P., Xu, W., Zhang, L. Q., Mao, S. X., Hudak, N. S., Liu, X. H., & Subramanian, A. (2010). In situ observation of the electrochemical lithiation of a single SnO2 nanowire electrode. *Science, 330*(6010), 1515-1520.
[31] Kimura, Y., Niinomi, H., Tsukamoto, K., & García-Ruiz, J. M. (2014). In situ live observation of nucleation and dissolution of sodium chlorate nanoparticles by transmission electron microscopy. *Journal of the American Chemical Society, 136*(5), 1762-1765.
[32] Lin, Y., Mallin, D., Chien, J., & Winter, H. (1991). Dynamic mechanical measurement of crystallization-induced gelation in thermoplastic elastomeric poly (propylene). *Macromolecules, 24*(4), 850-854.
[33] Panyukov, S., & Rabin, Y. (1996). Polymer gels: frozen inhomogeneities and density fluctuations. *Macromolecules, 29*(24), 7960-7975.
[34] Coviello, T., Burchard, W., Geissler, E., & Maier, D. (1997). Static and dynamic light scattering by a thermoreversible gel from Rhizobium leguminosarum 8002 exopolysaccharide. *Macromolecules, 30*(7), 2008-2015.
[35] Tanaka, F. (1990). Thermodynamic theory of network-forming polymer solutions. 2. Equilibrium gelation by conterminous crosslinking. *Macromolecules, 23*(16), 3790-3795.
[36] Kobayashi, K., Huang, C.-i., & Lodge, T. P. (1999). Thermoreversible gelation of aqueous methylcellulose solutions. *Macromolecules, 32*(21), 7070-7077.
[37] Smith, P., Lemstra, P., Pijpers, J., & Kiel, A. (1981). Ultra-drawing of high molecular weight polyethylene cast from solution: III. Morphology and structure. *Colloid and Polymer Science, 259*(11), 1070-1080.
[38] Kim, P. Y., Ribbe, A. E., Russell, T. P., & Hoagland, D. A. (2016). Visualizing the dynamics of nanoparticles in liquids by scanning electron microscopy. *ACS nano, 10*(6), 6257-6264.
[39] Mansfeld, U., Hoeppener, S., & Schubert, U. S. (2013). Investigating the motion of Diblock copolymer assemblies in ionic liquids by in situ electron microscopy. *Advanced Materials, 25*(5), 761-765.
[40] Bradley, D., & Roth, G. (2007). Adaptive thresholding using the integral image. *Journal of graphics tools, 12*(2), 13-21.
[41] De Gennes, P.-G. (1979). *Scaling concepts in polymer physics*: Cornell university press.
[42] Tanaka, H., Hayashi, T., & Nishi, T. (1986). Application of digital image analysis to pattern formation in polymer systems. *Journal of Applied Physics, 59*(11), 3627-3643.
[43] Williams, D. B., Carter, C. B., Williams, D. B., & Carter, C. B. (2009). Amplitude contrast. *Transmission Electron Microscopy: A Textbook for Materials Science*, 371-388.
[44] Takahashi, Y., & Tadokoro, H. (1973). Structural studies of polyethers,(-(CH2) mO-) n. X. Crystal structure of poly (ethylene oxide). *Macromolecules, 6*(5), 672-675.

[45] Takahashi, Y., Sumita, I., & Tadokoro, H. (1973). Structural studies of polyethers. IX. Planar zigzag modification of poly (ethylene oxide). *Journal of Polymer Science: Polymer Physics Edition, 11*(11), 2113-2122.
[46] Strobl, G. (2007). The semicrystalline state. *The Physics of Polymers: Concepts for Understanding Their Structures and Behavior*, 165-222.
[47] Guenet, J.-M. (1992). *Thermoreversible Gelation of Polymers and Biopolymers*: Academic Press Inc.

For the Table of Contents

A poly(ethylene glycol)-ionic liquid gel network was visualized by transmission electron microscopy (TEM) and TEM tomography.

Satyam Srivastava, Alexander E. Ribbe, Thomas P Russell *, David A Hoagland*